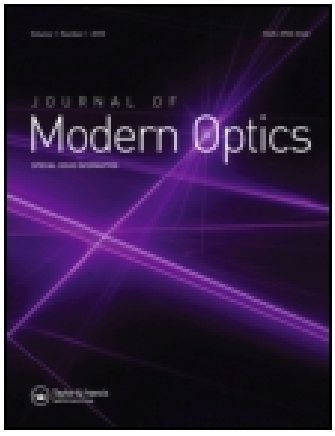

Journal of Modern Optics
Publication details, including instructions for authors and subscription information:
http://www.tandfonline.com/loi/tmop20

All-optical nonlinear plasmonic ring resonator switches

N. Nozhat[a] & N. Granpayeh[b]
[a] Faculty of Electrical Engineering, Shiraz University of Technology, Shiraz, Iran
[b] Faculty of Electrical Engineering, Center of Excellence in Electromagnetics, K. N. Toosi University of Technology, Tehran, Iran
Published online: 20 Aug 2014.

To cite this article: N. Nozhat & N. Granpayeh (2014) All-optical nonlinear plasmonic ring resonator switches, Journal of Modern Optics, 61:20, 1690-1695, DOI: 10.1080/09500340.2014.951008

To link to this article: http://dx.doi.org/10.1080/09500340.2014.951008

Journal of Modern Optics, 2014
Vol. 61, No. 20, 1690–1695, http://dx.doi.org/10.1080/09500340.2014.951008

All-optical nonlinear plasmonic ring resonator switches

N. Nozhat[a]* and N. Granpayeh[b]

[a]*Faculty of Electrical Engineering, Shiraz University of Technology, Shiraz, Iran;* [b]*Faculty of Electrical Engineering, Center of Excellence in Electromagnetics, K. N. Toosi University of Technology, Tehran, Iran*

(*Received 19 March 2014; accepted 28 July 2014*)

In this paper, all-optical nonlinear plasmonic ring resonator (PRR) switches containing 90° sharp and smooth bends have been proposed and numerically analyzed by the finite-difference time-domain method. Kerr nonlinear self-phase modulation (SPM) and cross-phase modulation (XPM) effects on the switching performance of the device have been studied. By applying a high-power lightwave, the signal can switch from one port to the other port due to the ON/OFF resonant states of the ring. We have shown that by utilizing the XPM effect, the output power ratio is improved by a factor of 2.5 and the required switching power is 31% of that of the case with only the SPM effect. Moreover, by utilizing sharp bend square-shaped ring resonators, the switching power is 10.4% lower than that of the smooth ones. The nonlinear PRR switches are suitable for application in photonic-integrated circuits as all-optical switches because of their nanoscale size and low required switching power.

Keywords: plasmonic ring resonator; nonlinear plasmonic switch; self-phase modulation (SPM); cross-phase modulation (XPM)

1. Introduction

Surface plasmon polaritons (SPPs) are the interaction of electromagnetic waves and the oscillations of electrons in metal, propagating on the metal-dielectric interfaces. SPPs are appropriate solutions for overcoming the diffraction limit and confining the electromagnetic lightwave in sub-wavelength scales [1–3]. Plasmonic devices based on SPPs are suitable for photonic-integrated circuits (PICs). Among various plasmonic waveguides, metal-dielectric-metal (MDM) structures have attracted much interests because of the high confinement of the lightwave, low bending loss, and acceptable propagation length [4]. Different passive MDM-based optical structures such as Multi-demultiplexers, couplers, tooth-shaped and stub waveguides, Bragg reflectors, nanocavities, Y-splitters, and Mach-Zehnder interferometers have been studied so far [5–10]. Due to the high optical field confinement of the SPPs, strong nonlinear effects can be achieved and so they can be used in active optical components [11–13].

Ring resonators have been used for many applications, such as wavelength and mode-selection, filtering, and wavelength multi-demultiplexing [1,14]. One of the considerable applications of ring resonators in the optical communication networks is switching, which can be achieved by nonlinear Kerr effects or other tunable procedures, such as thermo-optic, magneto-optic, and electro-optic effects [2,11,15–17]. Both circular and rectangular plasmonic ring resonators (PRRs) have been numerically or experimentally studied [16–24]. Also, some applications of ring/disk resonators, such as plasmonic channel add-drop filters have been investigated [25,26].

Compared to the circular ring resonators, rectangular-shaped ones have high coupling efficiency due to the long coupling section between the bus waveguide and the resonator [22]. Moreover, sharp bends in dielectric waveguides create a large bending loss, whereas plasmonic waveguides with bends can provide high transmission with low bending loss [14].

In this paper, we propose an all-optical switch based on nonlinear PRRs. Both 90° sharp and smooth bends are investigated. Nonlinear Kerr effect is used to control the light in our nanoscale PRRs. We employ self-phase modulation (SPM) and cross-phase modulation (XPM) Kerr effects to show the switching performance of the structures. The required switching powers for different states are compared. The sub-wavelength size and the low required pumping power of the PRR switch make it suitable for using in PICs.

The paper is organized as follows. In Section 2, the modeling and the analysis method and in Section 3, the simulation results of the nonlinear PRR switch containing sharp and smooth corner ring resonators are described and discussed. The paper is concluded is Section 4.

*Corresponding author. Email: nozhat@sutech.ac.ir

2. Geometry, modeling, and method of analysis

The schematic view of the PRR switch is shown in Figure 1. It consists of a sharp corner square-shaped PRR between two parallel straight waveguides. The parameters of the structure are the width of the waveguides and resonator (d), the gap between the waveguides and the resonator (g), and the side length of the ring resonator in the x (L_x) and z (L_z) directions.

The metal is silver and the dielectric in the waveguides and the ring resonator is chosen to be SiO_2 composite. The refractive index of the nonlinear dielectric is $n = n_0 + n_2 I$, where $n_0 = 1.47$ and $n_2 = 2.07 \times 10^{-9}\,(\mathrm{cm}^2/\mathrm{W})$ are the linear and nonlinear refractive indices, respectively, and I is the optical field intensity [15]. The dispersive dielectric function of the silver is described by the Drude model:

$$\varepsilon(\omega) = \varepsilon_\infty - \frac{\omega_P^2}{\omega^2 - j\gamma_P\omega}, \tag{1}$$

where $\varepsilon_\infty = 1.95$ is the relative permittivity at infinite frequency, $\omega_P = 1.37 \times 10^{16}\,(\mathrm{rad/s})$ and $\gamma_p = 20 \times 10^{12}\,(\mathrm{rad/s})$ are the plasma and collision frequencies, respectively [12]. The resonant wavelength of the rectangular ring resonator is determined by the equation:

$$Ln_{\mathrm{eff}} = m\lambda, \tag{2}$$

where m, an integer, is the mode number, $L = 2(L_x + L_z)$ is the effective length of the ring, n_{eff}, and λ are the ring effective refractive index and the free space wavelength, respectively. The effective refractive index of SPP modes for TM polarization can be obtained from the dispersion relation [11]:

$$\tanh\left(k_0 d\sqrt{n_{\mathrm{eff}}^2 - \varepsilon_d}\right) = -\frac{\varepsilon_d\sqrt{n_{\mathrm{eff}}^2 - \varepsilon_m}}{\varepsilon_m\sqrt{n_{\mathrm{eff}}^2 - \varepsilon_d}}, \tag{3}$$

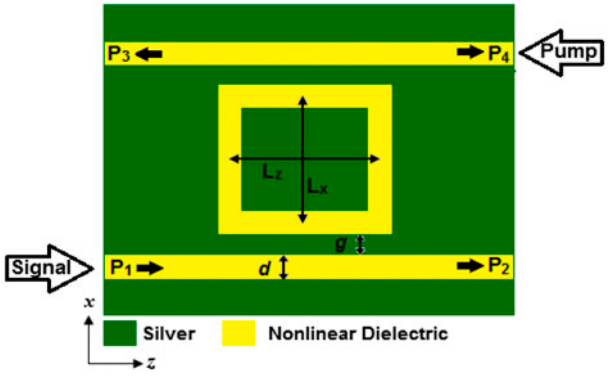

Figure 1. Schematic view of the PRR switch with sharp corners. (The colour version of this figure is included in the online version of the journal.)

where $k_0 = 2\pi/\lambda$ is the free space wave number, ε_d and ε_m are the dielectric constants of the dielectric and the metal, respectively.

We have used the two-dimensional finite-difference time-domain (2D-FDTD) numerical method with a convolutional perfectly matched layer (CPML) as absorbing boundary condition, to study the performance of our proposed nonlinear switch. The grid size of the FDTD cell in x and z directions are $\Delta x = \Delta z = 1\,\mathrm{nm}$ and the time step for numerical convergence due to Courant condition is $\Delta t = 0.95/\left(c\sqrt{(\Delta x)^{-2} + (\Delta z)^{-2}}\right)$, where c is the free space speed of light. Since the width of the waveguide is assumed much smaller than the operating wavelength, only the fundamental TM mode is supported.

3. Numerical results and discussion

3.1. The PRR switching performance by the SPM effect

The parameters of the square sharp corners PRR of Figure 1 is set to be d = 50 nm, and g = 20 nm, and $L_x = L_z$ = 570 nm. We have chosen these values to attain the ring resonant wavelength at 1535 nm. The incident wave is launched from P_1 at Figure 1. The transmittance at each port is attained by normalizing the power at each port to the input port power, P_1. The ON/OFF resonant conditions depend on the incident optical wavelengths, which would affect the phase interferences inside the ring. By solving the dispersion relation of Equation (3) for the PRR of Figure 1, the effective refractive index of the ring is attained to be $n_{\mathrm{eff}} = 2.028$ and so the resonant wavelengths of the ring can be calculated from Equation (2). A Gaussian pulse is launched to the input port, P_1, and the transmittance spectra at the

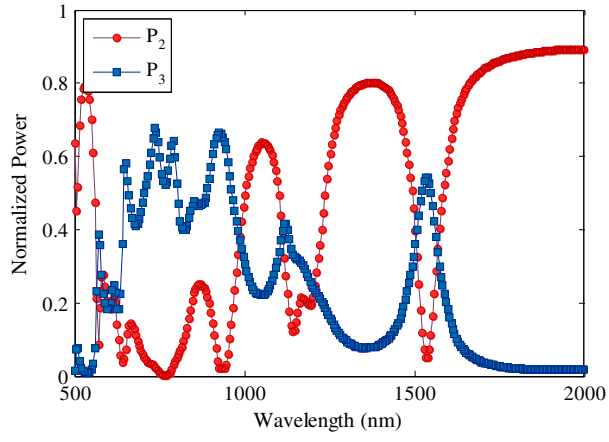

Figure 2. Transmittance spectra of the PRR switch with sharp corners of Figure 1, with $L_x = L_z$ = 570 nm, d = 50 nm, and g = 20 nm. (The colour version of this figure is included in the online version of the journal.)

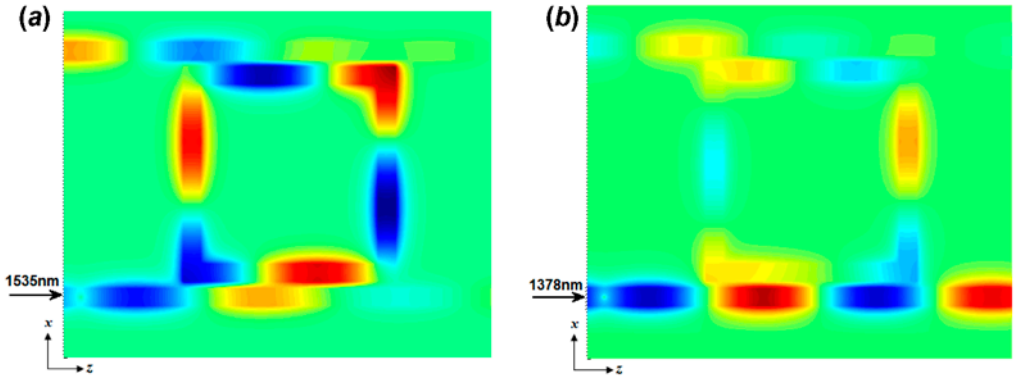

Figure 3. The magnetic field distributions of the PRR switch of Figure 1 at (*a*) ON resonant wavelength of 1535 nm and (*b*) OFF resonant wavelength of 1378 nm. (The colour version of this figure is included in the online version of the journal.)

output ports are depicted in Figure 2. Since the plasmonic structures have much higher loss compared to the dielectric ones, the transmission is not 100% compared to the dielectric ring resonators. The wavelength of 1535 nm in the third telecommunication window is one of the resonant wavelengths of the PRR. We consider this wavelength for studying the switching performance of the PRR.

The magnetic field distributions at ON/OFF states at the wavelengths of 1535 and 1378 nm are demonstrated in Figure 3. At the ON state, the incident wave couples to the ring and again couples to the left side of the upper waveguide and exits from P_3, so there is no wave at P_2 port. The magnetic field has six antinodes at the faces and corners of the square ring at the third resonant wavelength of 1535 nm (TM_3). In all wavelengths, some negligible lightwave exits uncontrollably from P_4 port.

To show the switching performance of the nonlinear PRR switch, a high-power CW signal at the wavelength of 1535 nm is launched to the input port P_1. By enhancing the input power, the refractive index of the dielectric ring resonator and so the resonant wavelength increase, hence the output power at the P_3 port decreases and the power exits from the P_2 port. The output power ratio, P_2/P_3, increases from −5.34 to 9.54 dB, when the input light intensity increases from 4.04×10^{-5} to 25.91 (MW/cm^2) by the self-phase modulation (SPM) effect, as shown in Figure 4. In the high-input intensity of 25.91 (MW/cm^2), corresponding to the optical power of 0.13 (KW/cm), the ring is at the OFF state and the wave exits from the P_2 port.

3.2. The PRR switching performance by the XPM Effect

In this Section, we study the effect of the XPM on the performance of our proposed switch. In general, the refractive index of the dielectric waveguide due to the Kerr nonlinear effect depends on the intensities of the signal, I_s, and pump, I_p:

$$n = n_0 + n_2\left(I_s + 2I_p\right), \tag{4}$$

where $n_2 I_s$ and $2n_2 I_p$ are the increment of the refractive index by the SPM and XPM effects, respectively.

From the transmittance spectra of Figure 2, we have chosen the pump wavelength of λ_p = 1504 nm that is the OFF state of the PRR. Two CW signals as the signal lightwave at λ_s = 1535 nm and the pump lightwave at λ_p = 1504 nm are simultaneously launched to the P_1 and P_4 ports, respectively. In the low pump intensity, the ring resonates at 1535 nm, so both of the signal and pump light exit from the P_3 port.

The magnetic field distribution of the pump lightwave is shown in Figure 5(*a*). By increasing the pump intensity, due to the Kerr XPM effect, the refractive

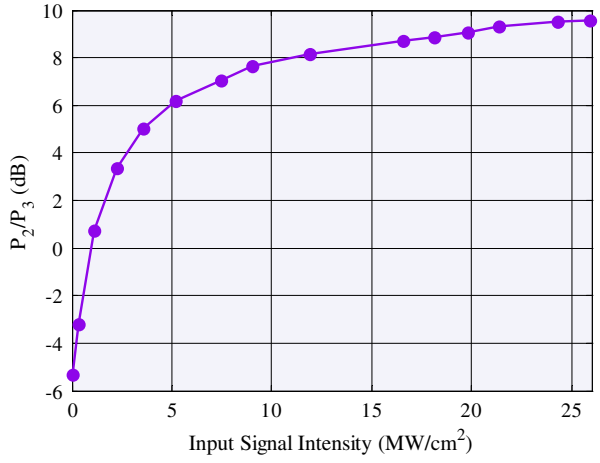

Figure 4. Output power ratio variations vs. the input signal intensity for the PRR switch of Figure 1 by the SPM effect. (The colour version of this figure is included in the online version of the journal.)

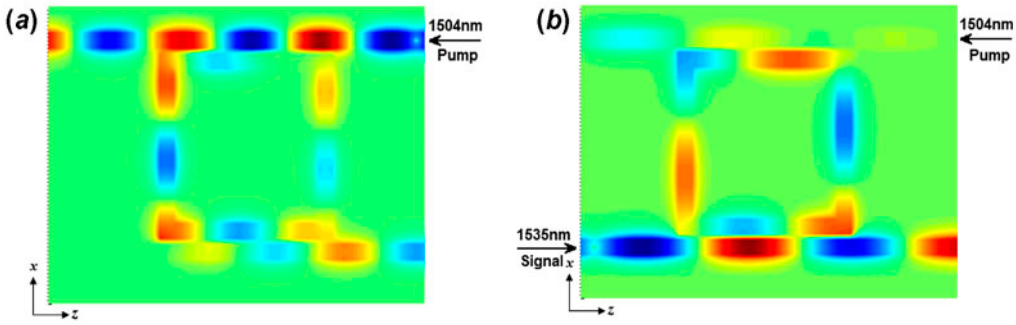

Figure 5. The magnetic field distributions of (*a*) the pump light at the wavelength of 1504 nm which is launched to the P_4 port and (*b*) the PRR switch in the nonlinear regime. The ring is at OFF condition and the signal lightwave exits from the P_2 port. The pump field distribution is not shown here. (The colour version of this figure is included in the online version of the journal.)

index of the ring increases according to Equation (4) and the resonant wavelength of the square ring increases. Therefore, the ring does not resonate at the signal wavelength of 1535 nm and the signal light exits from the P_2 port, while the pump light remains at the upper waveguide and exits from the P_3 port, as demonstrated in Figure 5(*b*). Since the intensity of the pump light in the nonlinear state is much larger than the signal light, the pump light field distribution is not shown in Figure 5(*b*). The output power ratio vs. the pump intensity is demonstrated in Figure 6.

By increasing the pump intensity from 4.04×10^{-5} to 8.07 (MW/cm^2), the power ratio changes from −5.34 to 23.6 dB. Compared to the case that only the Kerr nonlinear SPM effect has been considered, the output power ratio has been improved by a factor of 2.5. Moreover, the required light intensity for switching of the nonlinear PRR with Kerr XPM effect is 31% of the one with SPM effect.

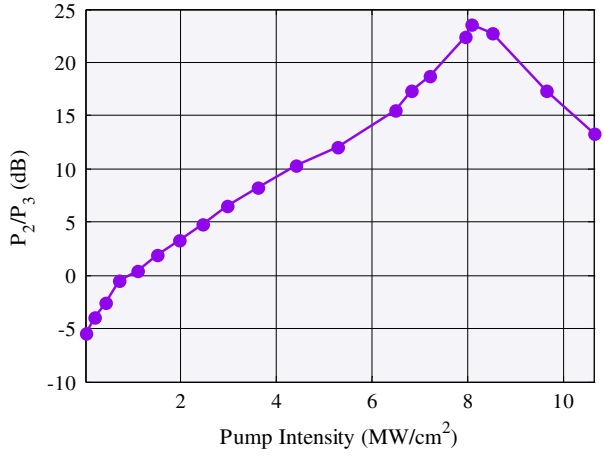

Figure 6. Output power ratio variations vs. the input pump intensity for the PRR switch of Figure 1 by the XPM effect. (The colour version of this figure is included in the online version of the journal.)

Next, we consider the switching performance of the PRR with 90° smooth corner bends as depicted in Figure 7. The length of the ring resonator in the x and z directions and the effective bend radius are $L_x = L_z = 590$ nm and $r = 75$ nm, respectively. These parameters are set to have the same resonant wavelength of the PRR with sharp corner bends. As shown in the transmission spectra of Figure 8, the wavelength of 1535 nm is one of the resonant wavelengths of the ring which the lightwave exits from the P_3 port.

To compare the switching power of the PRR switches with smooth and sharp corner bends by the XPM effect, signal and pump lightwaves at the wavelengths of $\lambda_s = 1535$ nm and $\lambda_p = 1504$ nm are simultaneously launched to the P_1 and P_4 ports, respectively. By increasing the pump intensity from 4.2×10^{-5} to 9.02 (MW/cm^2) the output power ratio increases from $P_2/P_3 = -3.1$ dB to $P_2/P_3 = 18.22$ dB, as illustrated in Figure 9 which the increment of the output power ratio is lower than that for the PRR switch with sharp corner bends, shown in Figure 6.

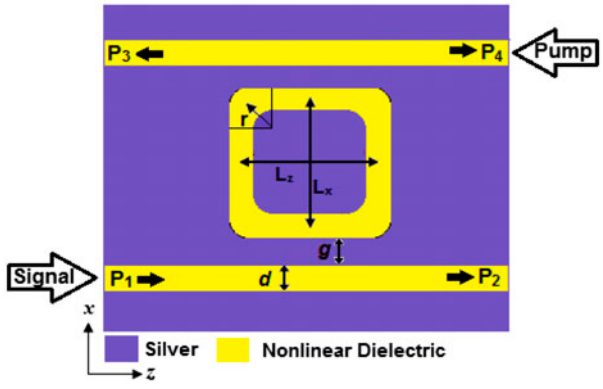

Figure 7. Schematic view of the PRR switch with smooth corner bends. (The colour version of this figure is included in the online version of the journal.)

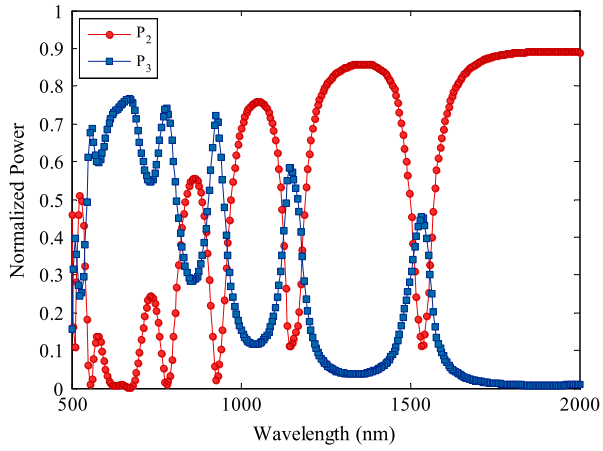

Figure 8. Transmittance spectra of the PRR switch with smooth corner bends of Figure 7, with $L_x = L_z = 590$ nm, $d = 50$ nm, $g = 20$ nm and bend radius of $r = 75$ nm. (The colour version of this figure is included in the online version of the journal.)

The dependence of the transmittance of the SPPs passing through a 90° bend MIM waveguide on the bending radius has been studied by Liu *et al.* [27]. When the bending radius is small, the loss is mainly caused by the reflection. The reflection and out-of-plane losses decrease as the bending radius increases. When the bending radius is large, the loss of the structure is mainly caused by the material loss. Thus, unlike the conventional dielectric waveguides, the transmittance through plasmonic structure bends decrease as the bending radius increases. As a result, the PRR switch with smooth corner bends requires more input switching power compared to the sharp bend one because of the higher metal loss.

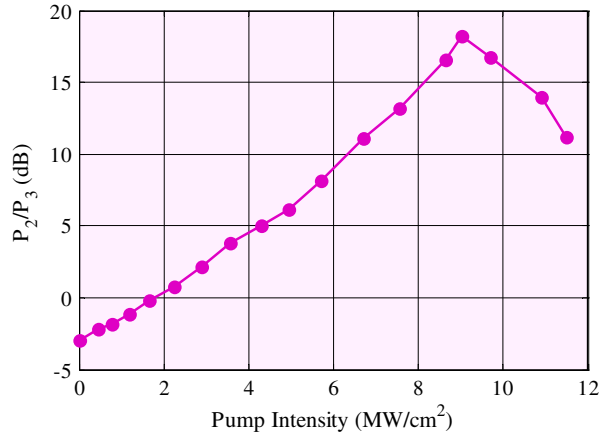

Figure 9. Output power ratio variations vs. the input pump intensity for the PRR switch of Figure 7 by the XPM effect. The increment of P_2/P_3 is lower than that for the PRR switch with sharp corner bends. (The colour version of this figure is included in the online version of the journal.)

The input pump intensity of the PRR switch with sharp corner bends is 10.4% lower than that with smooth bends. Moreover, the output power ratio in the PRR switch with sharp bends is 30% higher than that with smooth bends.

4. Conclusion

In this paper, the switching performance of a nonlinear plasmonic ring resonator (PRR) switch consisting of a square ring resonator between two parallel straight waveguides has been studied. The plasmonic switches with sharp and smooth corner bends have been considered. By applying the input lightwave in the low and high intensities, the ring resonator, filled with a Kerr nonlinear material, can be in the ON/OFF resonant conditions, respectively. Therefore, the nonlinear PRR can operate as an all-optical switch with sub-wavelength dimensions. It has been shown that using the Kerr nonlinear XPM effect, the required switching power of the PRR containing sharp bends is 69% lower than that with SPM effect, and the output power ratio is improved by a factor of 2.5. Furthermore, the switching power of the nonlinear PRR with 90° sharp corner bends is 89.6% of that with smooth corner bends by considering the Kerr nonlinear XPM effect.

References

[1] Hosseini, A.; Massoud, Y. *Appl. Phys.* **2007,** *90,* 181102.
[2] Mei, X.; Huang, X.G.; Jin, T. *Plasmonics* **2011,** *6,* 613–618.
[3] Peng, X.; Li, H.; Wu, C.; Cao, G.; Liu, Z. *Opt. Commun.* **2013,** *294,* 368–371.
[4] Zhou, X.; Zhou, L. *Appl. Opt.* **2013,** *52,* 480–488.
[5] Tao, J.; Huang, X.G.; Lin, X.; Zhang, Q.; Jin, X. *Opt. Express* **2009,** *17,* 13989–13994.
[6] Wang, B.; Wang, G.P. Appl. Phys. Lett. **2005,** *87,* 013107 (1–3).
[7] Nozhat, N.; Granpayeh, N. *Opt. Commun.* **2011,** *284,* 3449–3455.
[8] Wang, B.; Wang, G.P. *Opt. Lett.* **2004,** *29,* 1992–1994.
[9] Chen, J.; Li, Z.; Lei, M.; Fu, X.; Xiao, J.; Gong, Q. *Plasmonics* **2012,** *7,* 441–445.
[10] Zhang, Q.; Huang, X.G.; Lin, X.S.; Tao, J.; Jin, X.P. *Opt. Express* **2009,** *17,* 7549–7554.
[11] Zhong, Z.J.; Xu, Y.; Lan, S.; Dai, Q.F.; Wu, L.J. *Opt. Express* **2009,** *18,* 79–86.
[12] Nozhat, N.; Granpayeh, N. *IEEE Photon. Technol. Lett.* **2012,** *24,* 1154–1156.
[13] Nozhat, N.; Granpayeh, N. *Opt. Commun.* **2012,** *285,* 1555–1559.
[14] Chung, S.Y.; Wang, C.Y.; Teng, C.H.; Chen, C.P.; Chang, H.C. *J. Lightwave Technol.* **2012,** *30,* 1733–1742.
[15] Tao, J.; Wang, Q.J.; Huang, X.G. *Plasmonics* **2011,** *6,* 753–759.
[16] Randhawa, S.; Lacheze, S.; Renger, J.; Bouhelier, A.; Lamaestre, R.E.; Dereux, A.; Quidant, R. *Opt. Express* **2012,** *20,* 2354–2362.

[17] Reiserer, A.A.; Huang, J.S.; Hecht, B.; Brixner, T. *Opt. Express* **2010,** *18,* 11810–11820.
[18] Han, Z.; Van, V.; Herman, W.N.; Ho, P.T. *Opt. Express* **2009,** *17,* 12678–12684.
[19] Wang, T.B.; Wen, X.W.; Yin, C.P.; Wang, H.Z. Opt. Express **2009,** *17,* 24096–24101.
[20] Setayesh, A.; Mirnaziry, S.R.; Abrishamian, M.S. *J. Opt. Soc. Korea* **2011,** *15,* 82–89.
[21] Zand, I.; Mahigir, A.; Pakizeh, T.; Abrishamian, M.S. *Opt. Express* **2012,** *20,* 7516–7525.
[22] Zand, I.; Abrishamian, M.S.; Berini, P. *Opt. Express* **2013,** *21,* 79–86.
[23] Foroughi Nezhad, V.; Abaslou, S.; Abrishamian, M.S. J. Opt. **2013,** *15,* 055007 (1–7).
[24] Sederberg, S.; Driedger, D.; Nielsen, M.; Elezzabi, A.Y. *Opt. Express* **2012,** *19,* 23494–23503.
[25] Xiao, S.; Liu, L.; Qiu, M. *Opt. Express* **2006,** *14,* 2932–2937.
[26] Chu, H.S.; Akimov, Y.; Bai, P.; Li, E.P. *Opt. Lett.* **2012,** *37,* 4564–4566.
[27] Liu, L.; Han, Z.; He, S. *Opt. Express* **2005,** *13,* 6645–6650.